

Article

New Data on Autoionizing States of Ne Induced by Low-Energy Electrons from 45 to 64 eV

Jozo J. Jureta ¹, Bratislav P. Marinković ^{1,*}  and Lorenzo Avaldi ²¹ Institute of Physics Belgrade, University of Belgrade, Pregrevica 118, 11080 Belgrade, Serbia; jureta@ipb.ac.rs² CNR-Istituto di Struttura della Materia, Area della Ricerca di Roma 1, CP10, 00015 Monterotondo Scalo, Italy; lorenzo.avaldi@ism.cnr.it

* Correspondence: bratislav.marinkovic@ipb.ac.rs; Tel.: +381-11-3160882

Abstract: The lowest single and doubly excited autoionizing states of neon have been studied using a non-monochromatic electron beam and a high-resolution electrostatic analyzer at incident electron energies from 43.37 to 202 (± 0.4) eV at three ejection angles, 40°, 90° and 130°. The $2s2p^63s(3^1S)$ and $2s2p^63p(3^1P)$ as well as the $2p^43s3p$ doubly excited states have been observed and their energy determined. The influence of the PCI effect in the energy region of the $2s2p^63s(3^1S)$ states has been investigated. New features in the ejected electron spectra in the low kinetic energy region 3–20 eV at 202 eV incident energy have been observed and assigned.

Keywords: autoionization; neon; low-energy electrons; post-collision interaction

1. Introduction

Neon abundance in the cosmic scale of elements' abundances is relatively high, since it is created through stellar nucleosynthesis in massive stars [1]. Through the process of neutron capture [2] or electron capture, the neon inside certain massive stars may cause their collapse into a neutron star and produce a supernova [3]. Its presence in the solar photosphere [4] and the magnesium to neon (Mg/Ne) and neon to oxygen (Ne/O) abundance ratios in the Sun [5] also have profound implications on our understanding of the solar structure and evolution [6]. Data studies on neon electronic states include neutral neon atoms [7,8], and singly [9,10] and doubly [11] charged neon ions. Regarding electron scattering data from neutral neon atoms there exists the large scale pseudostate calculation [12] as well as the revisited generalized oscillator strengths of the valence shell excitations from the ground state [13].

In the past, autoionizing states of neon have been studied mostly at high energies by many authors using photons, electrons and ions as excitation source, c.f. Jureta et al. [14] and references therein. Experimental studies with low-energy electrons are scarce. The works by Comer and Read [15], Tahira et al. [16], Sharp et al. [17], Wilden et al. [18], Mitchell et al. [19] and van den Brink et al. [20] using both ejected and scattered electrons [15] or either ejected electrons [16–18] or scattered electrons [19,20] aimed to obtain the energies of the triplet/singlet states and to study the influence of the post-collision interaction (PCI) effect observed in the 3s states.

In the present work, we continue our investigation of the autoionizing states of rare gases [14,21–24] at low incident electron energies and high resolution in the analyzer. Here, the aim is to investigate the behavior of the Ne 3s and 3p singly excited states in two different modes of spectrometer operation, analyzing the ejected spectra as a function of incident energies limited to 64 eV, an energy between the $Ne^{2+} 2p^4(3^1P_2, 1^1D_2)$ ionization potentials at 62.53 eV and 65.73 eV, respectively, and at three ejected angles (40°, 90°, 130°). The influence of the PCI effects on the shape and energy shift of the $2s2p^63s(3^1S)$ states as a function of excess energy above their thresholds is also investigated. In addition, due to the high sensitivity and efficiency of the analyzer equipped with seven channeltrons, it was



Citation: Jureta, J.J.; Marinković, B.P.; Avaldi, L. New Data on Autoionizing States of Ne Induced by Low-Energy Electrons from 45 to 64 eV. *Atoms* **2024**, *12*, 6. <https://doi.org/10.3390/atoms12020006>

Academic Editor: Emmanouil P. Benis

Received: 6 December 2023

Revised: 15 January 2024

Accepted: 18 January 2024

Published: 23 January 2024



Copyright: © 2024 by the authors. Licensee MDPI, Basel, Switzerland. This article is an open access article distributed under the terms and conditions of the Creative Commons Attribution (CC BY) license (<https://creativecommons.org/licenses/by/4.0/>).

possible to detect and analyze several new features in the 3–13 eV kinetic energy region at 202 eV incident energy. These features are identified as the decay from the $\text{Ne}^+ 2s^2 2p^4 n l$ and $2s^1 2p^5 n l$ satellites to $\text{Ne}^{2+} ({}^3P_{0,1,2}, {}^1D_2, {}^1S_0)$. Also, it was possible to identify and precisely measure the energy of the first doubly excited $2s^2 2p^4 3s^2 ({}^3P)$ state and to identify a few doubly excited states with mixed $3s3p$ configuration in the ejected electron spectra.

2. Experiment

The experimental setup has been described in detail in [21], so only a brief overview will be given here. In the present experiment, a non-monochromatic beam of electrons with energies from 43.37 eV to 202 eV (defined with an uncertainty of ± 0.4 eV) collides perpendicularly with an atomic beam emerging from a platinum–iridium non-biased needle (I.D. 0.5 mm). The interaction region (I.D. 50 mm) is made by two cylinders of thin μ -metal foils with a separation of 10 mm in the collision plane, in order to avoid the collection of electrons scattered from metal surfaces.

The ejected electrons, after passing a high-resolution hemispherical analyzer with a mean radius of 125 mm, are detected by seven channeltrons. The analyzer operates at pass energy mode of 1 eV with a defined retarding ratio and a defined magnification determined by the two-stage 11 elements lens system. All spectra in these measurements are obtained in two operation modes of the spectrometer: the constant analyzer energy (CAE) and the constant retarding ratio (CRR) mode. In the CAE mode, the analyzer pass energy is constant, while the kinetic energy is scanned by varying the retarding ratio of the lens stack. In this way, the energy resolution is constant. In the CRR mode, the ratio of the kinetic energy E_k to the pass energy E_p ($K = E_k/E_p$) during the scan is constant ($K = E_k/E_p$), i.e., the ejected electrons are retarded by the lens stack by a constant proportion of their kinetic energy. The CAE mode provides a constant transmission and, thus, it enables the comparison of the intensity of the different peaks, while the CRR mode gives a better resolution.

The background and working pressure were 6×10^{-8} and 2×10^{-6} mbar, respectively. With an electron current of 10^{-6} A, a typical accumulation time for most of the spectra, with an energy step of 0.020 eV per channel, was about 30 min, depending of the ejection angle. The best resolution of the measured peaks was 0.045 (± 0.02) eV full width at half maximum (FWHM). All spectra are presented with subtracted background using a linear function without any further normalization of the obtained data. The reference for calibration of the kinetic energy scale was the energy position of the $\text{Ne } 2s^2 2p^5 3p ({}^1P)$ state at 24.00 eV, while the incident electron energy scale was calibrated using the elastic channel with an FWHM of about 0.80 eV.

3. Results and Discussion

3.1. The $2s2p^6 3s ({}^3,1S)$ and $2s2p^6 3p ({}^3,1P)$ States

Great attention has been focused in the past on determining the energies of the $2s2p^6 3s ({}^3,1S)$ states since they appear as an asymmetric broad peak in both energy loss and ejected spectra [15,17,19,20]. In [15,17], only the energy of the $2s2p^6 3s ({}^1S)$ state at 43.67 eV was given. In [19,20], the energies of both the $2s2p^6 3s ({}^3,1S)$ states were determined to be 43.59 and 43.67 eV, respectively.

In the present work, we investigated the ejected electron spectra of the $\text{Ne } 2s2p^6 3s ({}^3,1S)$ and $2s2p^6 3p ({}^3,1P)$ states obtained at several electron incident energies from 60 down to 45 eV (Figures 1–4). All the spectra were calibrated versus the energy position of the $2s2p^6 3p ({}^1P)$ state [14]. The lifetime of this excited state, which corresponds to an energy width of $\Gamma \approx 13$ meV [25], is so long that its energy position and shape in the spectrum do not vary due to PCI effects when the incident energy approaches its excitation threshold.

In Figures 1–3, the first broad intense structure represents the $2s2p^6 3s ({}^3,1S)$ states obtained in the CAE and CRR operation modes at ejection angles of 40° , 90° and 130° . The width and shape of this feature vary with the incident energy and the ejection angle. For example, the width increases from 170 meV to 380 meV in Figure 1a and from 180 meV to 420 meV as the incident energy decreases in Figure 1a,b, respectively. A Beutler–Fano

profile is also clearly seen in Figures 2 and 3 until 45 eV of incident energy. The 3s/3p intensity ratio shows an energy and angle dependence, too. At 50 eV the ratios are 1.05 at 40° in the CAE operation mode, and 0.82 and 0.43 at 40° and 130°, respectively, in the CRR operation mode. Since the shape and energy positions of the $2s2p^63s(^3,1S)$ states are very sensitive to experimental conditions, in Figure 4 we present the features due to the $2s2p^63s(^3,1S)$ and $2s2p^63p(^3,1P)$ states in the form of isolated structures obtained at the best resolution. Figure 4 shows the spectrum measured at 50.44 eV over the kinetic energy region 21.6–24.4 eV in the CRR operation mode at 40°, and the two isolated features due to the $2s2p^63s(^3,1S)$ and $2s2p^63p(^3,1P)$ states obtained with the best resolution of 45 meV with a 10 meV energy step, in order to resolve the components of the 3s states.

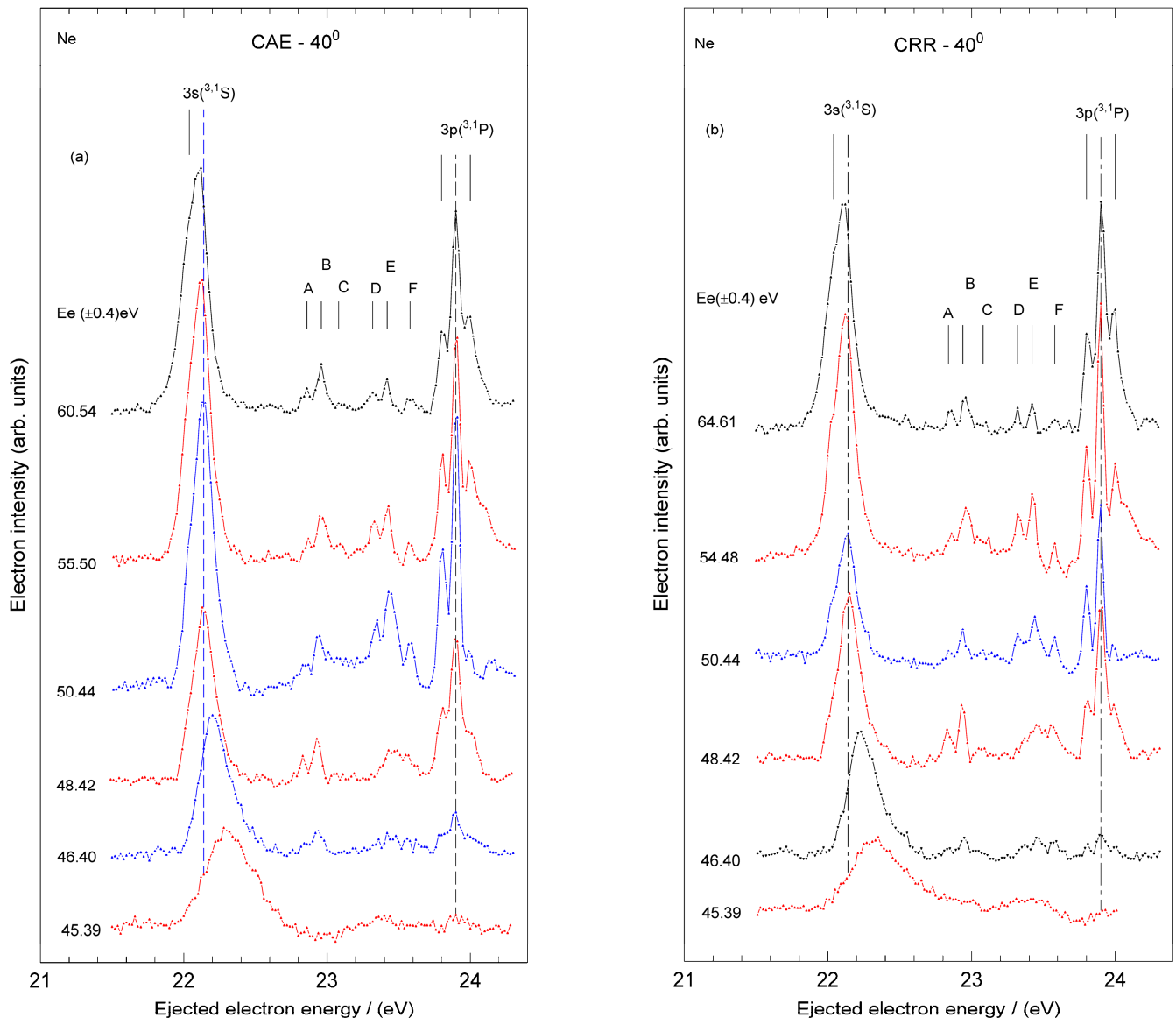


Figure 1. Spectra of Ne autoionizing states obtained in the (a) CAE; (b) CRR operation modes in the kinetic energy region 21.6 eV to 24.4 eV at 40° ejection angle. Electron incident energies (E_e) vary from 45.39 eV to 60.54 (± 0.4) eV in (a) and 45.39 eV to 64.61 eV in (b). The long dashed and short full lines denote the energy positions of the PCI unshifted $2s2p^63s(^3,1S)$ and the $2s2p^63p(^3,1P)$ states. The other short vertical lines labeled A–F indicate the 3s3p doubly excited states.

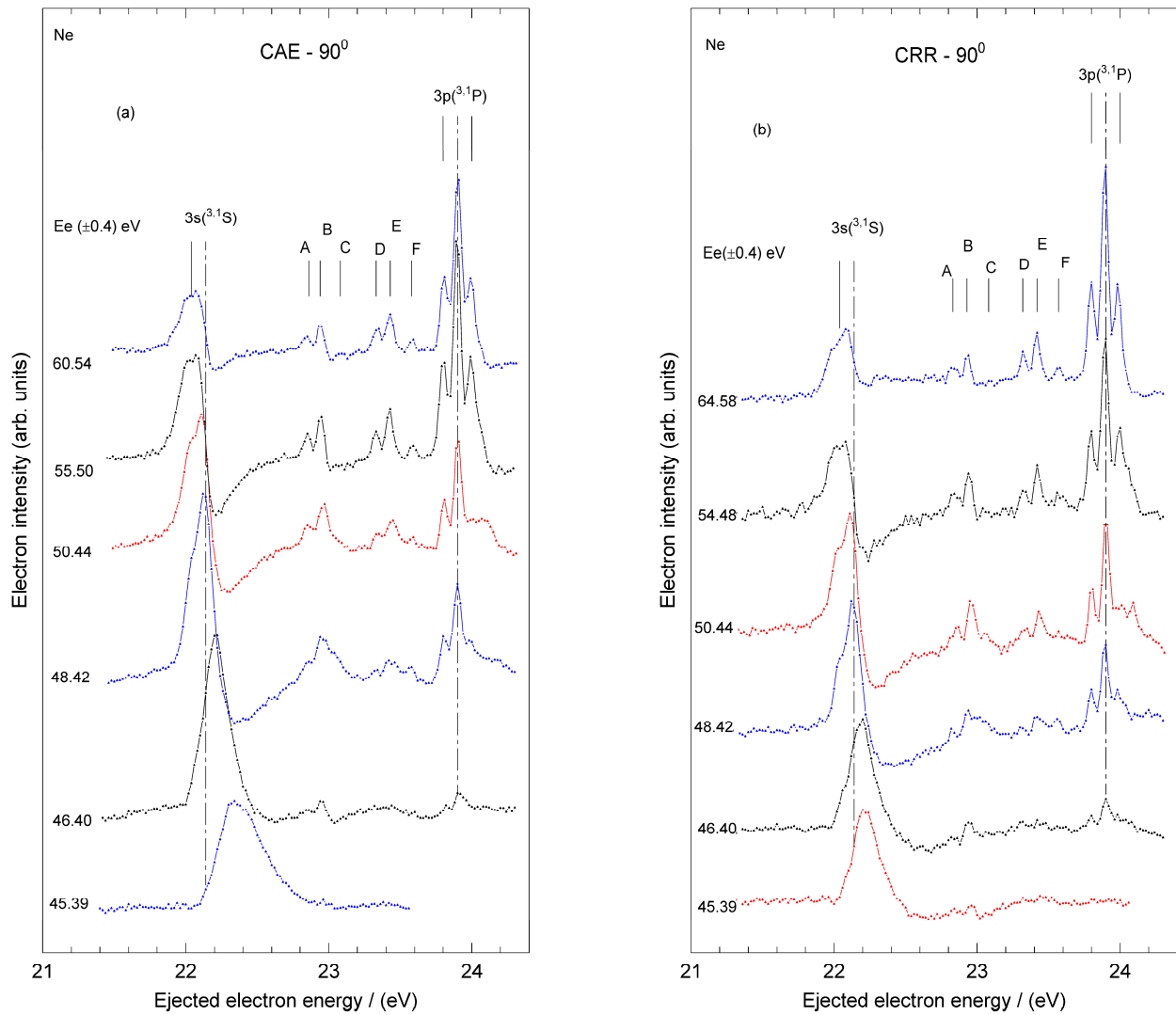


Figure 2. Spectra of Ne autoionizing states obtained in the (a) CAE; (b) CRR operation modes in the kinetic energy region 21.6 eV to 24.4 eV at 90° ejection angle. Electron incident energies (E_e) vary from 45.39 eV to 60.54 (± 0.4) eV in (a) and 45.39 eV to 64.61 eV in (b). The long dashed and short full lines denote the energy positions of the PCI unshifted $2s2p^63s(^3S)$ and the $2s2p^63p(^3P)$ states. The other short vertical lines labeled A–F indicate the $3s3p$ doubly excited states.

Both the triplet and singlet s and p states can decay to the two ion cores $2p^5 \text{Ne}^+ 2P_{3/2,1/2}$, which are separated by about 100 meV and should have a relative intensity of 2 to 1. Thus, each feature is composed of four peaks. In the 3p state, the separation between the peaks is larger than their natural linewidth; thus, the different peaks can be separated by a high-resolution experiment. We observe three peaks because the decay of the $3p\ ^3P$ neutral state to the $2P_{3/2}$ ion one overlaps with the decay of the $3p\ ^1P$ neutral state to the $2P_{1/2}$ ion one. The FWHM of the peak at 23.90 eV is 45 meV, which, considering the natural width of 13 meV, gives an experimental resolution of about 40 meV. Three peaks were also observed in [17,20], but not in [19]. The energy of the $3p(^1P)$ state at 45.54 eV is only defined in optical measurements [25] and it has been used as a calibration energy in [15,17,19,20]. However, only the energy of the $3p(^3P)$ state has been determined at 45.45 eV and 45.46 eV from ejected electron and energy loss experiments, respectively, in [17,19]. At higher incident energies [14,26], the energies of these states have been determined to be 45.46 eV and 45.44 eV, respectively. The absence of the third peak at higher incident energies should be noted [14]. Thanks to the high resolution (Figure 4) that is similar to the one in [17], it is possible to make a comparison of the two spectra. It is clear that the shapes of the 3p states and kinetic energies are almost identical.

The first peak in [17] is at 23.79 eV kinetic energy, while in the present work it is at 23.80 eV. The second and the third peaks are at 23.89 eV and 23.98 eV in [17] and 23.90 and 24.00 in the present work. In [17], the energy of the $3p(^3P)$ state was calculated as a mean value between the first and the second peak $(23.79 + 21.66) = 45.45$ eV and $(23.89 + 21.56) = 45.45$ eV, where 21.66 eV and 21.56 eV are the energy of the $Ne^+ 2p^5 (^2P_{3/2,1/2})$ states, respectively. In the present work, the energy of the $3p(^3P)$ state is obtained to be 45.46 eV $(23.80 + 21.66)$, $(23.90 + 21.56)$, where 23.80 eV and 23.90 eV are the observed kinetic energies of the first and second peak, respectively. The energy of the $3p(^1P)$ state in the present work is 45.56 eV $(23.90 + 21.66)$, $(24.00 + 21.56)$ to be compared with the 45.54 eV in [17]. The energies and assignments of the autoionizing singly excited $2s$ states are presented in Table 1 where the energies are compared with other data from the literature. A comparison with other references in Table 1 shows very good agreement with [15,17,19,20]. The spin-orbit splitting from the present work is around 100 meV, close to the 93 meV proposed in [19].

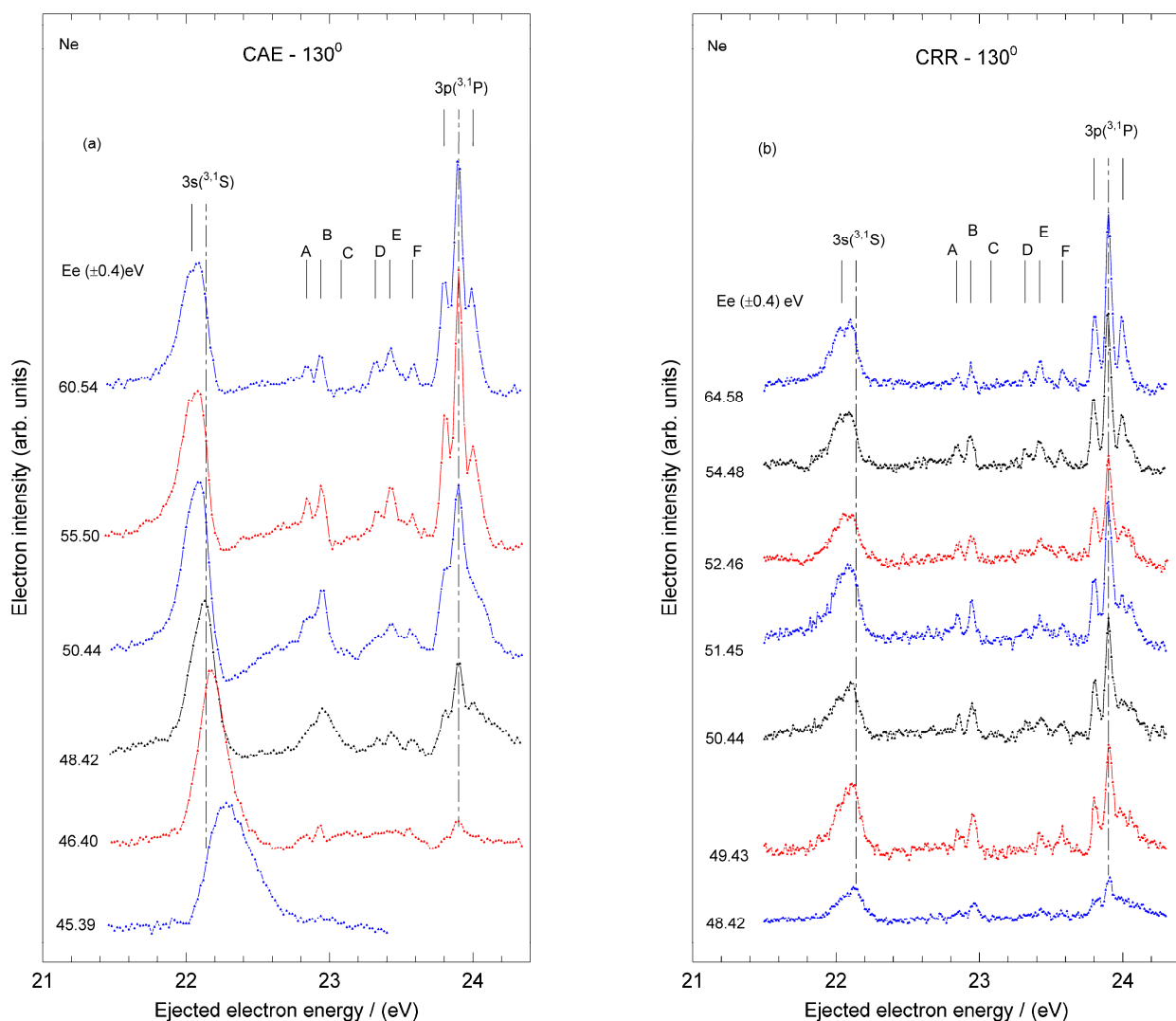


Figure 3. Spectra of Ne autoionizing states obtained in the (a) CAE; (b) CRR operation modes in the kinetic energy region 21.6 eV to 24.4 eV at 130° ejection angle. Electron incident energies (E_e) vary from 45.39 eV to 60.54 (± 0.4) eV in (a) and 45.39 eV to 64.61 eV in (b). The long dashed and short full lines denote the energy positions of the PCI unshifted $2s2p^63s(^3,1S)$ and the $2s2p^63p(^3,1P)$ states. The other short vertical lines labeled A–F indicate the $3s3p$ doubly excited states completely resolved. The spectra shown in (b) are obtained at the highest resolution (55 meV) in the CRR operation mode above 48 eV where the influence of the PCI effect is expected to be negligible.

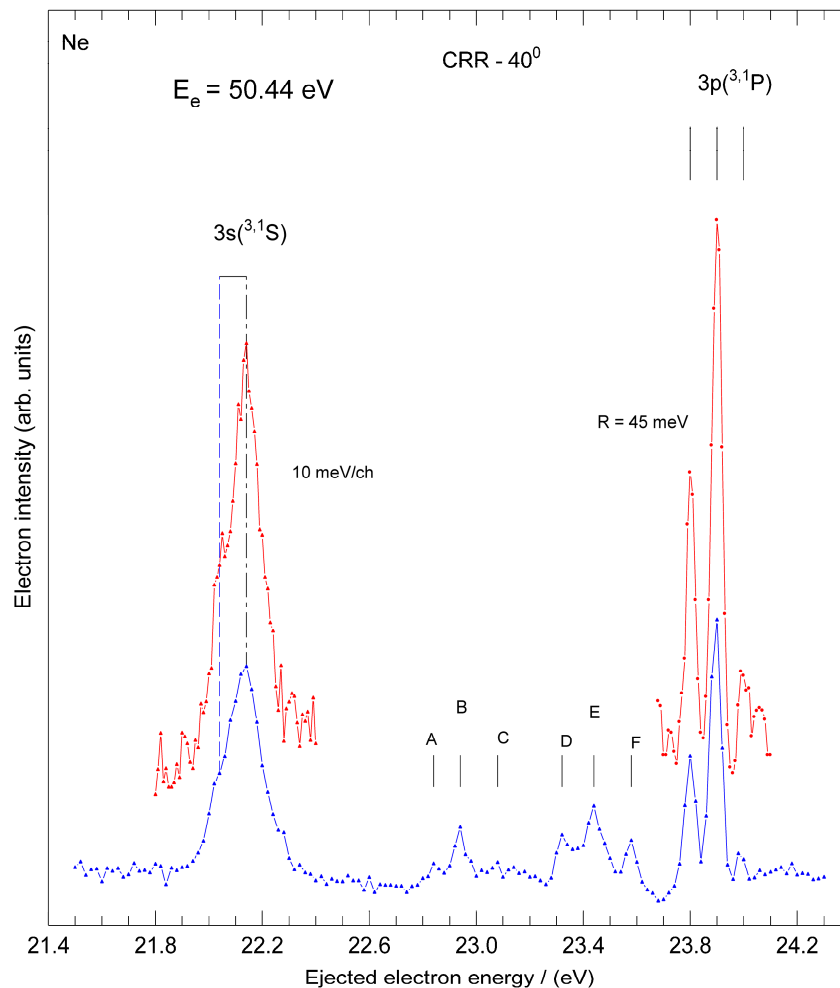


Figure 4. The Ne autoionizing spectrum obtained at an incident energy of 50.44 eV, i.e., 6.74 eV above the excitation energy of the $3s(^3,1S)$ states. The bottom spectrum is the same as in Figure 1b with a 20 meV energy step. The two insets show the regions of the $3s(^3,1S)$ and $3p(^3,1P)$ states measured with higher resolution and statistics and a 10 meV energy step. The resolution is 45 meV, measured as FWHM of the 3p states. The short vertical lines labeled A–F indicate the $3s3p$ doubly excited states.

Table 1. Kinetic energy, KE(eV), and excitation energies, (eV) *, of the autoionizing states of neon obtained from excitation of the 2s electron to the $2s2p^6(3s, 3p)$ singly excited states in the ejected energy region from 22.04 eV to 24.0 eV. References: Jureta et al. [14], Comer and Read [15], Sharp et al. [17], Mitchell et al. [19], van den Brink et al. [20], Codling et al. [25], Edwards and Rudd. [26].

This Work KE (eV)	Reference	Exc. En. (eV) *	Assignment
22.04	This work, Ee = 50 eV [14,19,20,26]	43.60 * (43.60 *, 43.59 *, 43.59 *, 43.41 *)	$2s2p^63s(^3S)$
22.14	This work, Ee = 50 eV [14,15,17,19,20]	43.70 * (43.70 *, 43.64 *, 43.67 *, 43.67 *, 43.67 *)	$2s2p^63s(^1S)$
23.80 23.90	This work, Ee = 50 eV [14,15,17,19,26]	45.46 * (45.46 *, 45.45 *, 45.45 *, 45.46 *, 45.44 *)	$2s2p^63p(^3P)$
23.90 24.00	This work, Ee = 50 eV [14,15,17,19,25]	45.56 * (45.56 *, 45.55 *, 45.54 *, 45.55 *, 45.546 *)	$2s2p^63p(^1P)$

The observed FWHM of the 3s feature is 210 meV. Even with 40 meV experimental energy resolution and the natural linewidths from the literature (80, 90 meV) [15,17,19]

for the ($^3,^1S$) states, the different components of the 3s state could not be resolved. This is mainly due to the influence of the PCI effect at low incident energies and the presence of negative ion resonances which can populate these autoionizing states [18]. We accept the energy of the 3s states from our previous work at a high incident energy [14] of 43.70 eV as a mean energy from kinetic energies of 22.04 eV and 22.14 eV in decay to the doublet term of the ion core (21.66, 21.56) eV. This value was attributed to the singlet $2s2p^63s(^1S)$ state, which means that the tabulated value of 43.60 eV for the triplet state is correct, if we accept the spin–orbit splitting of 100 meV.

Analyzing the spectrum at a low incident energy of 50.44 eV (Figure 4), the 3s states are present again in the form of a broad unresolved peak with a maximum at 22.14 eV and a shoulder on the lower energy side, at 22.04 eV, indicated by dashed lines, which gives a mean energy of 43.70 eV. This energy should be attributed to the $2s2p^63s(^1S)$, although its intensity should be lower than the intensity of the $3s(^3S)$ state at low incident energies. A comparison with other references in Table 1 shows a good agreement for both 3s states. The spin–orbit splitting of 100 meV is in good agreement with value of 80 meV predicted by [19].

It should be noted that in the energy loss measurements of [20], the authors have proposed that the broadening of the 3s states is due to state–state and state–continuum interference and the PCI effect. At a constant energy loss of 43.67 eV, i.e., the excitation energy of the $3s(^1S)$ state, they noticed a significant difference in the shape of the peak that was explained by a state–state interference effect because energies of the scattered and ejection electrons were equal. They also detected a minor effect due to the interference between the singly excited 1S state and the doubly excited autoionizing states.

3.2. The Post-Collision Interaction (PCI)

The broadening and shift of the feature assigned to the $3s(^1S)$ in Figures 1–3 is attributed to the PCI effect. The PCI effect corresponds to an interaction in the continuum between the scattered and ejected electrons. A slow receding scattered electron can modify the Coulomb field, felt by the faster, autoionizing, ejected one. This results in a shift in the energy position and change in the shape of the autoionizing peaks in the spectrum. The PCI effect is also dependent on the lifetime of the autoionizing state that determines the time of emission of the ejected electron. This effect is clearly visible up to about 5 eV above the excitation threshold of the $3s(^1S)$, and is angle-dependent. The energy shift, $E_{sh.}$, is a function of excess energy, ΔE , i.e., the energy difference between the incident electron energy and the ionization energy of the $3s(^1S)$ state, $E_{sh.} \propto \Delta E^\beta$, where the coefficient β is the free parameter in the fit [24].

We have chosen the results obtained in the CAE operation mode to analyze how the position of the peak changes with the excess energy from the threshold. The experimental shifts for the three ejected angles are presented in the log–log plot of Figure 5 where they are also compared with the angle-integrated results of [18]. Despite the measured shifts at the three scattering angles overlapping within their uncertainties, the separate fits to the three sets results in different β values: -1.9 ± 0.2 and -2.5 ± 0.2 at 40° and 90° – 130° , respectively. This is due to the dependence of the PCI on the relative angle between the ejected and low-energy scattered electrons. The global fit to all data gives $\beta = -2.4 \pm 0.3$. This value is different from the one obtained in [18] where the parameter is $\beta = -1.2$. The combined fit to the present data and the ones reported in [18] gives $\beta = -1.68 \pm 0.3$.

In summary, from Figure 5 different exponents are determined for the present data and those in [18,27], and both sets of data are represented by exponents different from the value of -0.5 predicted by [28,29] in helium. Determination of energy shift versus excess energy is quite sensitive to a precise determination of the excess energy and it depends on the energy and angular resolution of the experiment. The experiment of Wilden et al. [18] is characterized by a better energy resolution in the electron gun (80 meV), while in our case a non-monochromatic electron gun was used. The data of Wilden et al. have been taken at 40° , and our data at 40° , although characterized by absolute shifts different from

the ones measured in [18], display a similar exponent. The reason to perform a fit for the combined set of data is to try to see if a general trend can be individuated.

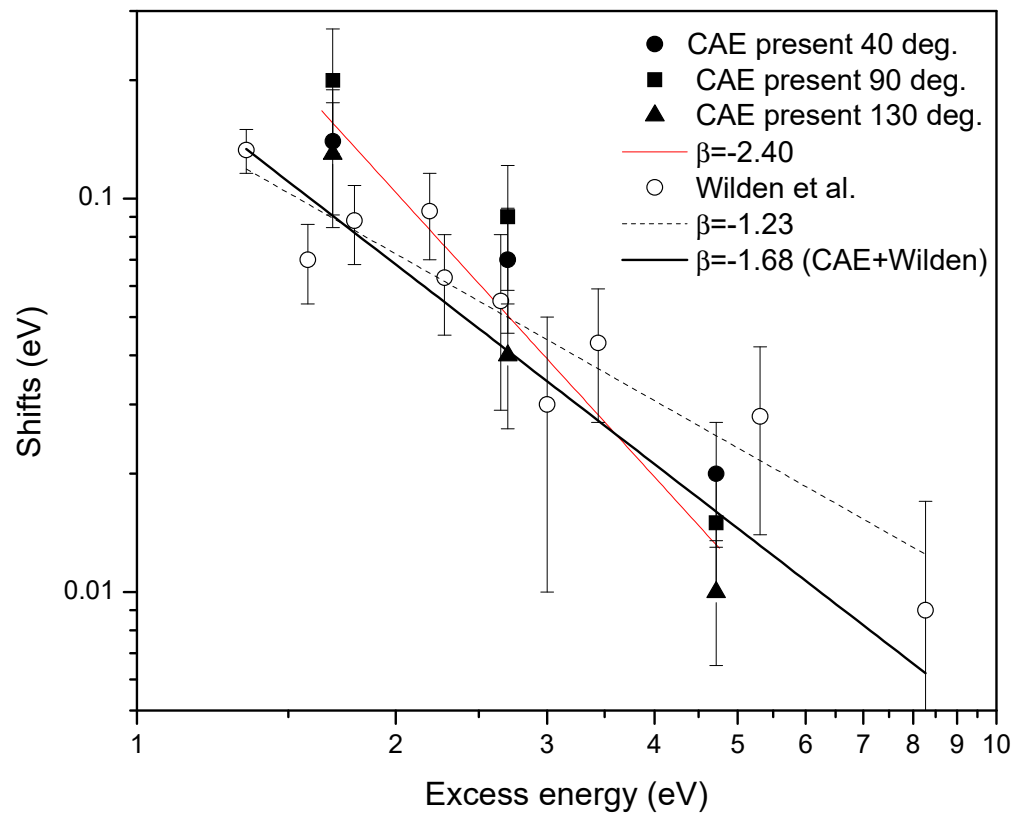


Figure 5. Log–log plot of the measured energy shift of the $3s(^3\text{1S})$ states versus the excess energies above the threshold at 43.70 eV at three ejection angles, 40° (full circles), 90° (full squares) and 130° (full triangles), compared with the data from [18] (open circles). The best fit of present data gives an exponent of $\beta = -2.4$ (thin solid red line), while the exponent in [18] (with the publisher’s permission to reproduce data points in Figure 2 from the source of the material by [18] © IOP Publishing. Reproduced with permission. All rights reserved.) is $\beta = -1.2$ (dashed line). A fit of the combined present data and the data in [18] gives $\beta = -1.68$ (thick solid line).

We note that we studied the PCI influence on the broad, unresolved structure of the $3s(^3\text{1S})$ state. The analysis is less precise and it cannot be directly compared with the one for helium, where the PCI effect is studied on the $2s^2(^1\text{S})$ state that appears as a single isolated peak. Also, the last broad structure at 45.39 eV incident energy is taken into account as a result of a strong PCI effect due to its energy position very close to the threshold. Its width is unusually large and its position is close to the energy position of the broad structure seen in [19] in an energy loss experiment at an energy around 44 eV with a width of 800 meV, assigned as the $2p^4(^3\text{P})3s3p$. A comparison between the two structures shows a difference in their widths (220–420) meV to 800 meV [19], while the energies are close (43.76–43.92) eV to 44 eV [19]. This structure has been seen in [30,31], at about 43.95 eV and assigned to a doubly excited state, and in [17], where the authors proposed its origin as the $2s2p^63s(^1\text{S})$ state displaced by 0.3 eV due to the PCI effect. In the present work, we accept this last approach and assign this feature to the $3s(^1\text{S})$ state.

3.3. The First Doubly Excited $2s^22p^43s^2(^3\text{P})$ State

The first doubly excited $3s^2(^3\text{P})$ state in the Ne autoionizing spectra has been observed previously, but its energy position has not been determined with high precision. The first unpublished calculation by A. Weiss gave a value of 42.2 eV, and then Grissom et al. [30] found the energy of this state to be 42.10 eV with the trapped-electron technique. Bolduc

and Marmet [31], via the examination of the electron ionization curves, found an energy of 42.22 eV. Both threshold techniques are affected by an unknown contribution of the PCI effect. A systematic study using the constant energy-loss technique with high energy resolution in both the incident electron beam and the analyzer, and a discussion on the previous investigations has been performed by Wilden et al. [18]. These authors gave an energy for the $3s^2(^3P)$ state of 41.87 eV and a width of about 0.1 eV.

In Figure 6, we present a new series of measurements in the 19.6–24.4 eV kinetic energy region and incident electron energies from 43.37 eV to 93.87 eV, i.e., from 1.39 eV to 51.89 eV above the excitation energy of the state, in order to cover a broad energy region for the PCI effects concerned.

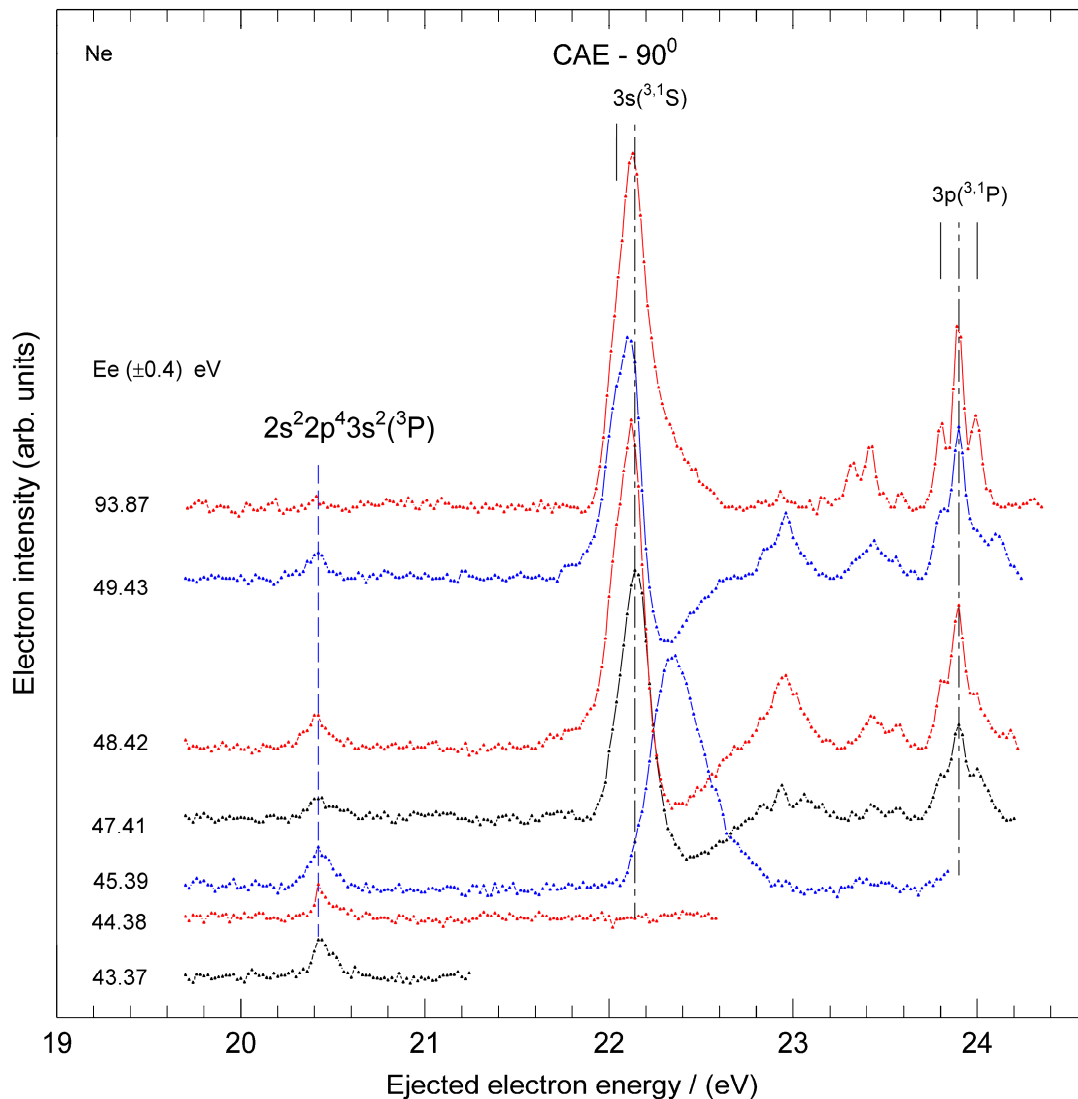


Figure 6. Series of autoionizing spectra of neon in the kinetic energy region from 20 eV to 24.4 eV obtained in the CAE mode at 90° from incident electron energies from 43.37 eV to 93.87 eV.

For the calibration of the kinetic energy scale, the energy of the $3p(^1P)$ state was used. The figure clearly shows that the feature assigned to the $3s^2(^3P)$ state does not display any shifts as the incident energy decreases, while this is not a case for the $3s(^3,1S)$ states. The energy of the feature is found to be 41.98 eV ($20.42 + 21.56$) with a width of approximately 0.15 eV. The figure shows that the intensity of the feature rises as the incident energy gets closer to its threshold. Some discrepancies are found in comparison with other works, where the energy of this state was different from our value by -0.11 , $+0.12$ and

+0.24 eV [18,30,31], respectively. In [18], the displacement of the state in an energy region near its threshold was noticed, but a definitive conclusion was not offered, suggesting a new measurement with a high-intensity signal. Wilden et al. [18] considered that if the $3s^2(^3P)$ state has its own structure, $^3P_{0,1,2}$, then the decay can populate the $Ne^+ 2s^2 2p^5(^2P_{3/2,1/2})$ states which are 100 meV apart; thus, the differences may be due to different population of the final states. Moreover, they performed a Rydberg analysis to justify the given energy. Another explanation for these discrepancies is the influence of the negative ion resonance reported in [32] at an energy of 42.09 eV. In the present measurements, where the ejected spectra are measured at incident energies above 43 eV, these resonances cannot be observed.

3.4. The Doubly Excited 3s3p Region

In Figures 1–3, several features, labeled A, B, C, D, E and F, with relative intensities depending of the ejection angle and incident energies, are visible between the $3s(^1S)$ and $3p(^1P)$ states. The six features are clearly observed at incident electron energies above 46 eV, while below that energy the PCI-shifted and -broadened feature of the $3s(^1S)$ state hampers their observation. The characteristic of the features is their independence from the PCI effect and energy separation. The features (A, B) at 22.84 eV and 22.94 eV and (D, E) at 23.32 eV and 23.44 eV have an energy separation of 100 meV, which corresponds to the energy separation of two terms in the ion core, indicating that these features correspond to the decay of two autoionizing states which have a mean energy of 44.50 eV and 44.99 eV, respectively. These energies are in excellent agreement with the energy of the features (b) at 44.48 eV and (c) at 44.97 eV in [17]. The assignments proposed in [17,33] and shown in Table 2 are $2p^4(^3P)3s(^2P)3p(^3D^0)$ and $2p^4(^3P)3s(^2P)3p(^1P^0)$. The latter, in the grandparent model, is also indicated as $2p^4(^3P)[3s3p(^3P)](^1P)$. The measured energies are also in excellent agreement with the ones of [25,31].

Table 2. Kinetic energy, KE(eV), and excitation energies, (eV) *, of the autoionizing 3s3p doubly excited states in the ejected energy region from 20.42 eV to 23.58 eV. References: Comer and Read [15], Sharp et al. [17], Wilden et al. [18], Codling et al. [25], Grissom et al. [30], Bolduc et al. [31] and Wills et al. [33].

This Work Label	KE (eV)	Reference	Exc. En. (eV) *	Assignment
	20.42	This work, [18,30,31]	41.98 * (41.87 *, 42.10 *, 42.04 *)	$2s^2 2p^4(^3P)3s^2(^3P)$
(A) (B)	22.84 22.94	This work, [17], (b) [31], E	44.50 * 44.48 * 44.43 *	$2p^4(^3P)3s(^4P)3p(^3D^0)$ or $(^3P^0)$
(C)	23.08	This work	44.64 *	
(D) (E)	23.32 23.44	This work, [17,25], (c) [31,33], F	44.99 * (44.97 *, 44.98 *) (45.00 *, 44.981 *)	$2p^4(^3P)3s(^2P)3p(^1P^0)$ $2p^4(^3P)[3s3p(^3P)](^1P)$
(F)	23.58	This work, [15,17], (d)	45.14 * 45.12 *	$2p^4(^1D)3s^2(^1D)$ or $2p^4(^3P)3s(^2P)3p(^3P^0)$

The features (C, F) appear as independent features at energies of 23.08 and 23.58 eV, respectively. The feature (C) has not been seen in [17]. In the present experiment, it is observed only at certain incident energies in Figures 1 and 2 and ejection angles of 40° and 90° with low intensity. The corresponding excited state at an energy of 44.64 eV is not found in the NIST database [34] and is left without assignment. The energy of the feature (F) at 45.14 eV is in excellent agreement with energy of the feature labeled (d) at 45.12 eV in [15,17], with a proposed double assignment as $2p^4(^1D)3s^2(^1D)$ or $2p^4(^3P) 3s(^2P)3p(^3P^0)$ as shown in Table 2. A comparison between these measurements and our previous measurements at high incident energies [14] shows an excellent agreement between feature (d) at 23.44 eV in Figures 4 and 5 of [14] and the present feature (E). The energies and assignments of the autoionizing 3s3p doubly excited states are presented in Table 2 where the energies are compared with other data from the literature.

3.5. The Ejected Electron Energy Region from 3 to 21 eV

The autoionizing spectra of neon obtained at a 90° ejection angle in the CAE operation mode in the ejected energy region from 3 eV to 21 eV is shown in Figure 7. It is the first time that the region of the ejected electron energy below 12 eV is accessed in an electron impact experiment.

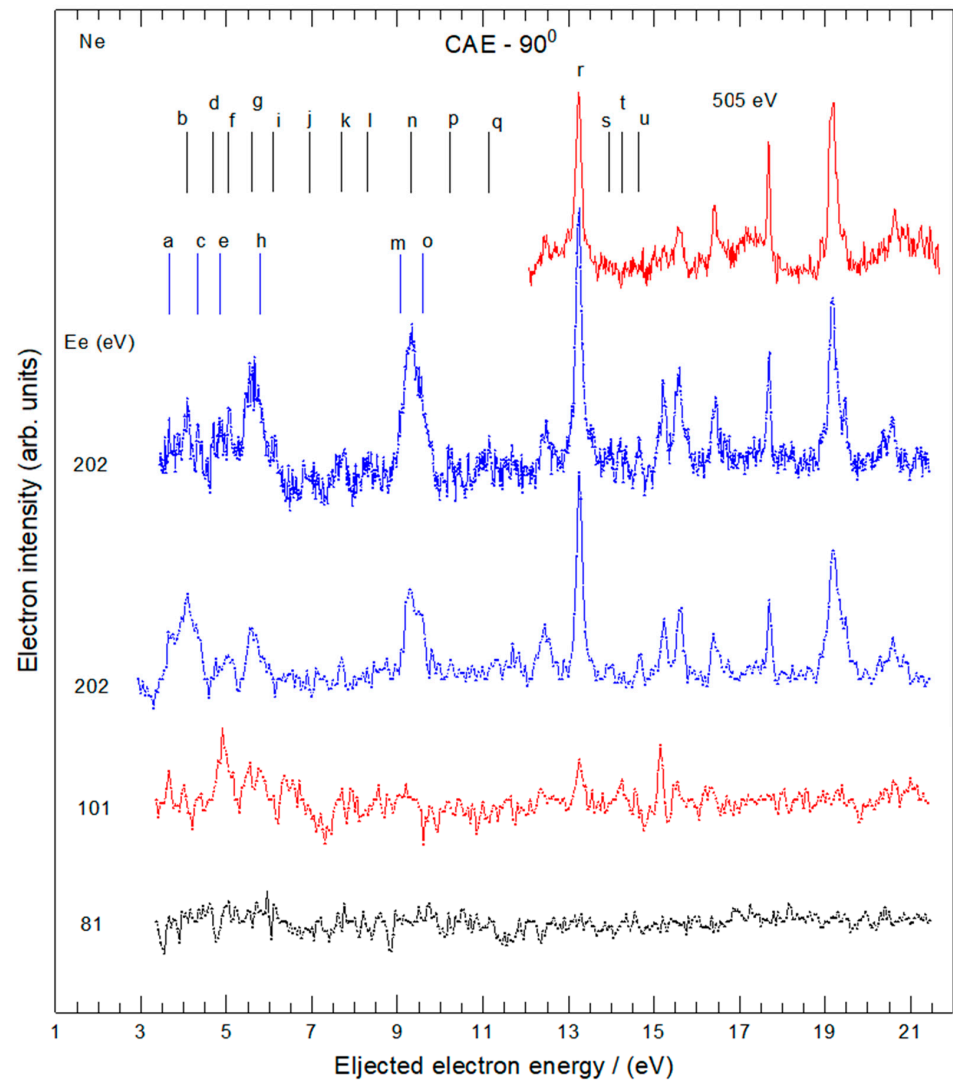


Figure 7. Series of autoionizing electron spectra due to the decay of the $2s^22p^4nl$ and $2s^12p^5nl$ satellite states in the kinetic energy region from 3 eV to 21 eV obtained at constant incident electron energies of 202 eV, 101 eV and 81 eV at 90° in the CAE mode. The spectrum at 202 eV at the top of the figure was accumulated with an energy step of 0.020 eV, while the three other spectra were accumulated with an energy step of 0.050 eV in order to achieve better statistics in shorter time. A part of the spectrum at the top of the figure, between 13 eV and 21 eV measured at 505 eV, has been analyzed in [14]. The short full lines labeled from (a) to (u) at the top of the figure indicate the kinetic energies of newly observed features.

The region of the spectrum above 13 eV kinetic energy shown at the top of Figure 7 at 505 eV incident energy was analyzed in [14]. The CRR operation mode used in that experiment did not allow to access the region below 13 eV. In the figure, the difference in the shape of the features in the two regions, broad unresolved features in the first part and narrow in the second part, both obtained in the same experimental conditions, has to be noted. The reason can be the larger number of the narrow lines in the first part not resolved in the present experiment, or a different origin of these features. The assignments of the

features above 12 eV kinetic energy in [14] were made according to their energies calculated as the sum of corresponding kinetic energies and three ionization potentials of Ne^{2+} (^3P , ^1D , ^1S) at 62.53 eV, 65.74 eV and 69.43 eV, respectively, [35], and in comparison with Edwards and Rudd [26] and Kikas et al. [36]. The assignment of the features below 12 eV kinetic energy is made here in the same way, but the comparison is made only with [36]. It should be noted that the ionization potentials of Ne^{2+} (^3P , ^1D , ^1S) used in [36] for the calculation of the energies for satellites are 62.7 eV, 65.9 eV and 72.8 eV, respectively, which differs by (0.17, 0.16, 3.37) eV from [35]. Table 2 shows the comparison of energies determined in this work and [14,34,36,37]. The assignments of the features proposed by [36], where the binding energies of the Ne^+ $2s^22p^4nl$, $2s^02p^6nl$ and $2s^12p^5nl$ excited satellite states have been tabulated, is accepted. In Table 3, a very good agreement in energies for features (b, c, d, g, h, k, n, q, r, s) and discrepancies for features (a, f) is observed. All other features are left without assignments due to the absence of data from previous studies.

Table 3. Kinetic energies, (KE) (eV), taken from Figure 7 and excited energies, (eV) *, of the $2s^22p^4nl$ and $2s^12p^5nl$ satellites calculated as a sum of ionization potentials of Ne^{2+} (^3P , ^1D , ^1S) (62.53, 65.74, 69.43) eV [35] and corresponding kinetic energies, respectively. References: Jureta et al. [14], Kramida et al. [34], Kikas et al. [36] and Svensson et al. [37].

Label	This Work KE (eV)	Reference	Exc. En. (eV) *	Assignment
(a)	3.66	This work, [36], Line 49	66.19 * 65.99 *	$2p^4(^1\text{S})4d(^2\text{D})$
(b)	4.08	This work, [36], Line 50	66.61 * 66.64 *	$2p^4(^1\text{S})5p(^2\text{P}^0)$
(c)	4.32	This work, [36], Line 51	66.85 * 66.78 *	(Tail of previous)
(d)	4.68	This work, [36], Line 52	67.21 * 67.26 *	$2p^4(^1\text{S})6s(^2\text{S})$
(e)	4.84	This work	67.37 *	
(f)	5.04	This work, [36], Line 53	67.53 * 67.61 *	$2p^4(^1\text{S})6p(^2\text{P}^0)$
(g)	5.58	This work, [36], Line 55	68.11 * 68.16 *	$2p^4(^1\text{S})7d(^2\text{D})$
(h)	5.78	This work, [36], Line 56	68.31 * 68.36 *	$2p^4(^1\text{S})8s(^2\text{S})$
(i)	6.10	This work	68.63 *	
(j)	6.94	This work	69.47 *	
(k)	7.70	This work, [36], Line 59	70.23 * 70.27 *	
(l)	8.30	This work	70.83 *	
(m)	9.08	This work	71.61 *	
(n)	9.32	This work, [36], Line 60 [37]	75.06 * 74.99 * 75.11 *	$2s^12p^5(^3\text{P})3s(^2\text{P})$
(o)	9.58	This work	75.32 *	
(p)	10.22	This work	75.96 *	
(q)	11.13	This work, [34]	76.87 * 76.85 *	$2s2p^5(^1\text{P}_1)$

Table 3. Cont.

Label	This Work KE (eV)	Reference	Exc. En. (eV) *	Assignment
(r)	13.24	This work, [14], (B) [36], Line 62 [37]	78.98 * 78.97 * 78.97 * 78.90 *	$2s^1 2p^5 (^3P) 3p (^2S)$
(s)	13.94	This work [36], Line 65 [37]	83.37 * 83.42 * 83.34 *	$2s^1 2p^5 (^3P) 4p (^2S)$
(t)	14.25	This work	83.68 *	
(u)	14.65	This work	84.08 *	

In order to visualize the energy levels of autoionizing states, we refer to the existing literature. The energy diagram has been provided by several authors: energy levels in the range from 42 eV to 50 eV for neutral Ne and Ne-ions are shown in Figure 4 of [38] and Figure 7 of [39]; the energy level diagram of observed and calculated Ne $2s^2 2p^4 3s 3l$ configurations for the $2s^2 2p^4 (^1S, ^1D, ^3P)$ and possible limits of Ne grandparent configurations in Figure 6 of [31]; the energy diagram of $2p^3 (^4S, ^2D, ^2P)nl$ Ne²⁺ ion configurations are shown in Figure 4 of [35]; the first- and second-step Auger decay paths for the $1s 2s (^3, ^1S) 3s 3p$ with $J = 1$ inner-shell doubly excited states of Ne are shown in Figure 2 of [40].

4. Conclusions

The autoionizing spectra of neon at low incident electron energies from 43.37 eV to 202 eV and three ejection angles (40° , 90° and 130°) have been studied by using a non-monochromatic electron beam and a high-resolution electrostatic analyzer. The influence of the PCI to the shape of the $2s 2p^6 3s (^3, ^1S)$ states was clearly observed, but the overlap of the $^3, ^1S$ states in one broad peak hampered a precise determination of the behavior of the PCI effects (shift and width of the peak) with excess energy. In addition, the energy position of the first doubly excited $2s^2 2p^4 3s^2 (^3P)$ state at 41.98 ± 0.02 eV, as well as the ones of the six features in the kinetic energy region between the $3s (^3, ^1S)$ and $3p (^3, ^1P)$ states produced by the $3s 3p$ doubly excited states, were determined. Also, in the low kinetic energy region of 3–13 eV at 202 eV incident energy, several new features identified as the decay of the Ne⁺ $2s^2 2p^4 nl$ and $2s^1 2p^5 nl$ satellite states are observed.

The focus of the present study is the spectroscopy of the autoionizing states of neutral neon atoms using low-energy electrons and three ejected angles. The obtained results open a perspective for new experiments in which the change in the shape of line profiles could be examined varying the ejected angles in small steps. Then, performing an analysis similar to the one performed in [41], one would be able to closely examine the role of direct ionization and autoionization. Both processes contribute to the electron profile resulting in Fano lineshapes. Then, the post-collision interaction of the projectile and the ejected electron will add up. It would be possible to record ejected electron spectra in steps of 5° or 10° to follow the changes in the profile. These kinds of interference lineshapes can be treated with Shore parametrization similarly to that performed in [21] for He atoms. An experimental upgrade of the electron spectrometer by replacing the existing electron gun with a monochromatic one could improve the data analyses.

Author Contributions: Conceptualization, J.J.J. and B.P.M.; methodology, J.J.J.; software, J.J.J. and B.P.M.; validation, J.J.J., B.P.M. and L.A.; formal analysis, J.J.J., B.P.M. and L.A.; investigation, J.J.J.; resources, J.J.J. and B.P.M.; data curation, J.J.J. and B.P.M.; writing—original draft preparation, J.J.J.; writing—review and editing, J.J.J., B.P.M. and L.A.; visualization, J.J.J., B.P.M. and L.A.; supervision, B.P.M. and L.A.; project administration, B.P.M. and L.A.; funding acquisition, B.P.M. and L.A. All authors have read and agreed to the published version of the manuscript.

Funding: This research was supported by the Science Fund of the Republic of Serbia, grant #6821, project name: “Atoms and (bio)molecules-dynamics and collisional processes on short time scale” (ATMOLCOL).

Data Availability Statement: Data are contained within the article.

Acknowledgments: The work has been performed within the Italy and Serbia bilateral project of particular relevance (Grande Rilevanza) “Nanoscale insights in radiation damage”. One of us, J.J.J., is grateful to the Institute of Physics Belgrade for being allowed to use their material resources.

Conflicts of Interest: The authors declare no conflicts of interest.

References

1. Prantzos, N.; Ekström, S. Stellar Nucleosynthesis. In *Encyclopedia of Astrobiology*; Gargaud, M., Amils, R., Quintanilla, J.C., Cleaves, H.J., Irvine, W.M., Pinti, D.L., Viso, M., Eds.; Springer: Berlin/Heidelberg, Germany, 2011; pp. 1584–1592. [\[CrossRef\]](#)
2. Nishimura, T.; Aikawa, M.; Suda, T.; Fujimoto, M.Y. Oxygen and Light-Element Synthesis by Neutron-Capture Reactions in Metal-Free and Extremely Metal-Poor AGB Stars. *Publ. Astron. Soc. Jpn.* **2009**, *61*, 909–929. [\[CrossRef\]](#)
3. Zha, S.; Leung, S.-C.; Suzuki, T.; Nomoto, K. Evolution of ONeMg Core in Super-AGB Stars toward Electron-capture Supernovae: Effects of Updated Electron-capture Rate. *Astrophys. J.* **2019**, *886*, 22. [\[CrossRef\]](#)
4. Asplund, M.; Grevesse, N.; Sauval, A.J.; Pat, S. The Chemical Composition of the Sun. *Annu. Rev. A&A* **2009**, *47*, 481–522.
5. Young, P.R. Element Abundance Ratios in the Quiet Sun Transition Region. *Astrophys. J.* **2018**, *855*, 15. [\[CrossRef\]](#)
6. Christensen-Dalsgaard, J. Solar structure and evolution. *Living Rev. Sol. Phys.* **2021**, *18*, 2. [\[CrossRef\]](#)
7. Chang, E.S.; Schoenfeld, W.G.; Birkmont, E.; Quinet, P.; Palmeri, P. Improved Experimental and Theoretical Energy Levels of Neon I. *Phys. Scr.* **1994**, *49*, 26–33. [\[CrossRef\]](#)
8. Saloman, E.B.; Sansonetti, C.J. Wavelengths, Energy Level Classifications, and Energy Levels for the Spectrum of Neutral Neon. *J. Phys. Chem. Ref. Data* **2004**, *33*, 1113–1158. [\[CrossRef\]](#)
9. Persson, W. The Spectrum of Singly Ionized Neon, Ne II. *Phys. Scr.* **1971**, *3*, 133–155. [\[CrossRef\]](#)
10. Kramida, A.E.; Nave, G. The Ne II spectrum. *Eur. Phys. J. D* **2006**, *39*, 331–350. [\[CrossRef\]](#)
11. Kramida, A.E.; Nave, G. New FTS measurements, optimized energy levels and refined VUV standards in the Ne III spectrum. *Eur. Phys. J. D* **2006**, *37*, 1–21. [\[CrossRef\]](#)
12. Zatsarinny, O.; Bartschat, K. Large-scale pseudostate calculations for electron scattering from neon atoms. *Phys. Rev. A* **2012**, *85*, 062710. [\[CrossRef\]](#)
13. Wang, S.-X.; Du, X.-J.; Sun, Q.; Liu, Y.-W.; Qi, D.-G.; Zhu, L.-F. Revisiting the oscillator strengths and cross sections of atomic neon by fast electron scattering. *J. Quant. Spectr. Rad. Transf.* **2022**, *277*, 107988. [\[CrossRef\]](#)
14. Jureta, J.J.; Marinković, B.P.; Milosavljević, A.R.; Avaldi, L. Singly and doubly excited states in ejected electron spectra of neon at high incident electron energies. *Eur. Phys. J. D* **2015**, *69*, 74. [\[CrossRef\]](#)
15. Comer, J.; Read, F.H. Electron impact studies of autoionizing states in neon and helium. *J. Electron. Spectrosc.* **1972**, *1*, 3–11. [\[CrossRef\]](#)
16. Tahira, S.; Nishimura, F.; Oda, N. Energy and angular distributions of electrons ejected from autoionization states in neon by electron impact. *J. Phys. B At. Mol. Phys.* **1973**, *6*, 2306–2309. [\[CrossRef\]](#)
17. Sharp, J.M.; Comer, J.; Hicks, P.J. Autoionizing transitions in neon studied by low-energy electron impact. *J. Phys. B At. Mol. Phys.* **1975**, *8*, 2512–2519. [\[CrossRef\]](#)
18. Wilden, D.G.; Hicks, P.J.; Comer, J. Electron impact studies of resonances and autoionizing states of neon. *J. Phys. B At. Mol. Phys.* **1977**, *10*, 1477–1486. [\[CrossRef\]](#)
19. Mitchell, P.; Baxter, J.A.; Comer, J. Electron energy-loss study of the $2s2p^63s$ and $2s2p^63p$ configurations of neon. *J. Phys. B At. Mol. Phys.* **1980**, *13*, 2817–2827. [\[CrossRef\]](#)
20. van den Brink, J.P.; den Outer, P.N.; van Eck, J.; Heideman, H.G.M. Coherence and correlation in electron impact autoionisation of neon and argon. *J. Phys. B At. Mol. Opt. Phys.* **1990**, *23*, 2349S–2362S. [\[CrossRef\]](#)
21. Paripás, B.; Jureta, J.J.; Palásthy, B.; Marinković, B.P.; Pszota, G. High resolution study of the autoionizing states of He in their exchange interference energy region. *J. Electron. Spectrosc. Relat. Phenom.* **2018**, *225*, 10–15. [\[CrossRef\]](#)
22. Avaldi, L.; Jureta, J.J.; Marinković, B.P. Energy analysis of ejected electrons in the region of the Ar $L_{1-2,3}M$ Coster-Kronig transitions (25–56 eV) induced by electron impact. *J. Electron. Spectrosc. Relat. Phenom.* **2019**, *237*, 146898. [\[CrossRef\]](#)
23. Jureta, J.J.; Marinković, B.P.; Avaldi, L. The $M_{4,5}$ -NN Auger and $M_{2,3}$ - $M_{4,5}N$ Coster-Kronig spectra of krypton induced by electron impact. *J. Quant. Spectrosc. Radiat. Transf.* **2021**, *268*, 107638. [\[CrossRef\]](#)
24. Jureta, J.J.; Marinković, B.P.; Avaldi, L. The $N_{4,5}$ -OO Auger and “ N_3 ”- $M_{4,5}O_{2,3}$ Coster-Kronig spectra of xenon induced by electron impact. *Adv. Space Res.* **2023**, *71*, 1338–1351. [\[CrossRef\]](#)
25. Codling, K.; Madden, R.P.; Ederer, D.L. Resonances in the Photo-Ionization Continuum of Ne I (20–150 eV). *Phys. Rev.* **1967**, *155*, 26–38. [\[CrossRef\]](#)
26. Edwards, A.K.; Rudd, M.E. Excitation of Auto-Ionizing Levels in Neon by Ion Impact. *Phys. Rev.* **1968**, *170*, 140–144. [\[CrossRef\]](#)

27. Smith, A.J.; Hicks, P.J.; Read, F.H.; Cvejanović, S.; King, G.C.; Comer, J.; Sharp, J.M. Phenomena associated with near-threshold excitation of autoionizing levels of helium by electron impact. *J. Phys. B At. Mol. Phys.* **1974**, *7*, L496–L502. [[CrossRef](#)]
28. Barker, R.B.; Berry, H.W. Electron Energy Distributions from Ionizing Collisions of Helium and Neon Ions with Helium. *Phys. Rev.* **1966**, *151*, 14–19. [[CrossRef](#)]
29. Hicks, P.J.; Cvejanović, S.; Comer, J.; Read, F.H.; Sharp, J.M. Displacements of electron ejection energies in near-threshold excitation of autoionizing levels of helium by electron impact. *Vacuum* **1974**, *24*, 573–580. [[CrossRef](#)]
30. Grissom, J.T.; Garrett, W.R.; Compton, R.N. Autoionizing and negative-ion states in neon. *Phys. Rev. Lett.* **1969**, *23*, 1011–1014. [[CrossRef](#)]
31. Bolduc, E.; Quemener, J.J.; Marmet, P. Autoionizing $2s^2 2p^4 3s 3l$ States of Ne and Related Ne^- Resonances. *J. Chem. Phys.* **1972**, *57*, 1957–1966. [[CrossRef](#)]
32. Buckman, S.J.; Clark, C.W. Atomic negative-ion resonances. *Rev. Mod. Phys.* **1994**, *66*, 539–655. [[CrossRef](#)]
33. Wills, A.A.; Cafolla, A.A.; Svensson, A.; Comer, J. Resonance structure in the neon photoelectron satellites. *J. Phys. B At. Mol. Opt. Phys.* **1990**, *23*, 2013–2028. [[CrossRef](#)]
34. Kramida, A.; Ralchenko, Y.; Reader, J.; NIST ASD Team. *NIST Atomic Spectra Database (Ver. 5.11)*; National Institute of Standards and Technology: Gaithersburg, MD, USA, 2023. Available online: <https://physics.nist.gov/asd> (accessed on 12 April 2023). [[CrossRef](#)]
35. Avaldi, L.; Dawber, G.; Gilley, N.; Rojas, H.; King, G.C.; Hall, R.; Stuhec, M.; Zitnik, M. A study of Ne^{2+} and Ar^{2+} satellite states observed by ‘threshold photoelectrons coincidence’ spectroscopy. *J. Phys. B At. Mol. Opt. Phys.* **1997**, *30*, 5197–5212. [[CrossRef](#)]
36. Kikas, A.; Osborne, S.J.; Ausmees, A.; Svensson, S.; Sairanen, O.-P.; Aksela, S. High-resolution study of the correlation satellites in photoelectron spectra of the rare gases. *J. Electron Spectrosc. Relat. Phenom.* **1996**, *77*, 241–266. [[CrossRef](#)]
37. Svensson, S.; Eriksson, B.; Mårtensson, N.; Wendin, G. Electron shake-up and correlation satellites and continuum shake-off distributions in X-Ray photoelectron spectra of the rare gas atoms. *J. Electron. Spectrosc. Relat. Phenom.* **1988**, *47*, 327–384. [[CrossRef](#)]
38. Roy, D.; Delage, A.; Carette, J.-D. Resonances in the differential excitation functions of five electronic states of Ne in the autoionization region. *Phys. Rev. A* **1975**, *12*, 45–51. [[CrossRef](#)]
39. Spence, D. A technique to enhance and separate negative ions from neutral autoionising features in scattered electron spectra in the ionisation continuum: Application to negative ions in neon. *J. Phys. B At. Mol. Phys.* **1980**, *13*, 1611–1624. [[CrossRef](#)]
40. Xiao-Bin, D.; Chen-Zhong, D.; Koike, F.; Kato, T.; Fritzsche, S. Excitation and decay dynamics of $1s2s$ inner-shell double-vacancy states of neon atoms. *Chin. Phys. B* **2008**, *17*, 592–598. [[CrossRef](#)]
41. Moretto-Capelle, P.; Benhenni, M.; Bordenave-Montesquieu, D.; Bordenave-Montesquieu, A. Distortion of He ($2l2l'$) Fano lineshapes by strong post-collision interaction in HC–He collisions. *J. Phys. B At. Mol. Opt. Phys.* **1996**, *29*, 2007–2020. [[CrossRef](#)]

Disclaimer/Publisher’s Note: The statements, opinions and data contained in all publications are solely those of the individual author(s) and contributor(s) and not of MDPI and/or the editor(s). MDPI and/or the editor(s) disclaim responsibility for any injury to people or property resulting from any ideas, methods, instructions or products referred to in the content.